

Exploring the Acoustics of the Chinese Transverse Flute (*dizi*)

Xinmeng Luan,^{1, a} Song Wang,¹ Gary Scavone,¹ and Zijin Li²

¹Computational Acoustic Modeling Laboratory, Center for Interdisciplinary Research in Music Media and Technology, Schulich School of Music, McGill University, Canada

²Department of Music AI, Central Conservatory of Music, China

(Dated: 10 September 2024)

We investigate the acoustical characteristics of the Chinese transverse flute, the *dizi*, employing input impedance measurements, modeling and analysis. The input impedances for various fingerings of a *bangdi* in the key of F, a particular type of the *dizi*, are measured and compared to models using both the transfer matrix method and the Transfer Matrix Method with external Interaction (TMMI). In order to get more accurate modeling results, we provide specific transfer matrices for the unique components of the *dizi*, such as back end-holes, membrane hole and upstream branch. The matching volume length correction for holes drilled in a thick wall is also derived. Comparative analysis of modeling and measurement data validates the improved accuracy of TMMI, confirming the influence of radiated sound from closely spaced toneholes.

[<https://doi.org/DOI number>]

[XYZ]

Pages: 1–11

I. INTRODUCTION

The *dizi*, a traditional Chinese transverse flute crafted primarily from bamboo, is most distinguished from the western flute by the presence of a hole covered by a wrinkled membrane. The wrinkled membrane is believed to contribute to the unique sound brightness of the *dizi*. Two traditional types of the *dizi* are the *qudi* and *bangdi*. The *qudi* accompanies operas like the *Kunqu* Opera in Southern China, while the *bangdi*, characterized by its shorter bore, is closely associated with the *bangzi* opera originating from Northern China.

The general shape of the *dizi*, shown in Fig. 1, is similar to that of the western flute, with a cylindrical bore and a series of toneholes along its length. The membrane hole is located between the embouchure hole and six downstream finger holes. Four extra end-holes are located near the bottom of the bore as follows: two axially distributed front end-holes, like the other toneholes along the front side, as well as two radially distributed back end-holes. Similar configurations of end-holes can also be found on the *Xiao*, a Chinese longitudinal flute. An internal cork, not visible externally, is located a short distance above the embouchure hole. Thus, the acoustically-relevant section of the instrument is from the cork to the downstream end. The section referred to as the “flute head” in Fig. 1 is not modeled in this study.

The unique component of the *dizi*, the membrane, is made from a thin film extracted from reed or bamboo

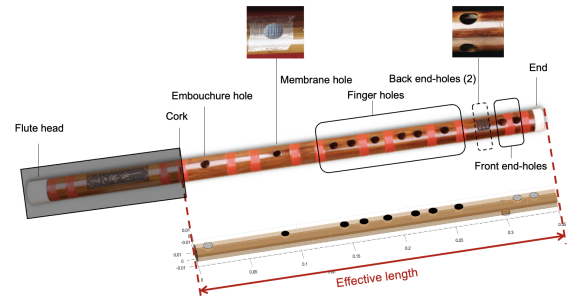


FIG. 1. General shape of the *dizi*.

stems, making it notably delicate and fragile. Its lifespan is short, typically lasting only a few months at most. There are various aspects that need to be taken into account when selecting a suitable membrane, such as the type of the *dizi*, playing techniques, and music style, as it significantly affects the instrument’s timbre. Before performing, the musician needs to manually create wrinkles on the membrane and attach it to the membrane hole. Furthermore, the method of attaching the membrane, its natural texture, and the formation of wrinkles, make a difference of tonal quality.

Selecting a high-quality *dizi* poses a challenge for professional musicians. Craftsmen encounter difficulties in achieving precise intonation in crafting a *dizi*, primarily due to the absence of scientific guidelines and heavy reliance on experience. Despite similarities in geometry between the *dizi* and the Western flute, nuanced distinctions contribute to the former’s distinctive acoustic char-

^axinmeng.luan@mail.mcgill.ca

acteristics. This study seeks to deepen our understanding of the *dizi*'s physics by undertaking modeling and analysis of its input impedance.

The physical principles that govern the production and radiation of sound by western musical instruments have been explained in detail in [Benade \(1990\)](#), [Rossing and Fletcher \(1991\)](#) and [Chaigne and Kergomard \(2016\)](#). However, there have been only a few scientific studies of Chinese musical instruments, with most of those coming in the 21st century. Some noteworthy contributions related to the *dizi* are as follows: [Tsai \(2003\)](#) made remarkable contributions to the study of the *dizi* from both a physics and perception perspective. He explained the importance of the tension and wrinkles in the membrane in producing a beautiful, bright *dizi* timbre. The non-linear behavior of the membrane was studied by modeling it as a Duffing oscillator. Wrinkling reduces the cubic non-linearity of the membrane, avoiding a jump phenomenon in its response curve compared to a slack and unwrinkled membrane. In another study, [Ng et al. \(2021\)](#) measured and analyzed the input impedance of the *dizi*.

Some studies about other Chinese wind instruments have been conducted. The input impedance of the *Xiao* was measured and modeled by the transfer matrix method and some optimization of the bore shape was suggested in [Lan and Waltham \(2016\)](#). [Kuang et al. \(2016\)](#) proposed the physical model and sound synthesis method of the *Sheng* in order to study the relationship between its physical structure and the timbre.

Toneholes are the distinguishing feature of woodwind instruments. The configuration and dimensions of finger holes on a wind instrument undergo meticulous refinement to achieve a harmonious balance in intonation and timbre across various fingerings. Employing input impedance as a pivotal tool for woodwind instrument analysis holds potential, as it provides information about both the magnitudes and harmonicities of resonances, along with identifying the cutoff frequency of the tonehole lattice. Moreover, leveraging input impedance analysis aids in evaluating the influence of subtle alterations in hole and bore geometries across different fingerings. Consequently, this study adopts an input impedance perspective to delve into the study of the *dizi*.

The Transfer Matrix Method (TMM) is a widely used approach for one-dimensional modeling of the air column of wind instruments ([Caussé et al., 1984](#); [Dickens, 2007](#); [Keefe and Douglas, 1990](#); [Plitnik and George, 1979](#); [Rucz et al., 2015](#)). We present a new application of the TMM, and the Transfer Matrix Method with external Interactions (TMMI) to the *dizi*, which, to the best of our knowledge, has not been attempted before. Some valuable numerical analysis results have already been reported in [Luan et al. \(2023\)](#). The impedance calculated from these methods can be compared with the measured data to justify the modeling. Additionally, it is worth mentioning that the *dizi* investigated in this study is an F-key *bangdi*. Prior to this, [Tsai \(2003\)](#) and [Ng et al. \(2021\)](#) conducted studies on the C-key *qudi* and G-key *bangdi*, respectively.

The paper is structured as follows. First, the measurement system and process are discussed in Sec. II. Then, the modeling details are extensively elaborated in Sec. III. Section IV presents the discussion of the analysis of the measurement and modeling results. Finally, Sec. V draws some final conclusions.

II. MEASUREMENT

A custom-build multi-microphone system based on a least-squares signal processing technique ([Lefebvre and Scavone, 2011](#); [Wang et al., 2021](#)) is used to measure the input impedance of the *dizi* (see Fig. 2). Six microphones are spaced along the impedance tube and three non-resonant loads are used to calibrate the apparatus, including a quasi-infinite impedance, an almost purely resistive impedance, and an unflanged pipe radiation load, similar to the description in [Dickens et al. \(2007\)](#) and [Kemp et al. \(2010\)](#).

The input impedance of each fingering is measured sequentially with and without the membrane. Blu-Tack is used to seal the toneholes and membrane hole. The fingerings corresponding to the measurements consisted of eight groups without half-holes (OXXXXX, XXXXXX, XXXXXO, XXXXOO, XXXOOO, XXOOOO, XOOOOO, OOOOOO) and five groups with half-holes (DOOOOO, XDoooo, XXDOOO, XXXXDO, XXXXXD), where O stands for open, X for closed and D for semi-closed, and the corresponding finger hole sequence starts from the upstream of the *dizi*. Fingerings without half-holes correspond to the first two octaves of the F-key *bangdi*, given by the diatonic notes C5 to B7. Note that for the *dizi*, as a convention, the tonic and dominant of the key is determined according to the fingering XXXOOO and OOOOOO, respectively. Additionally, half-holing is a common technique in playing the *dizi*, which is extremely useful for performing portamento and acciaccatura. There are likely to be discrepancies between the areas of the half-hole conditions in the measurements compared with normal performance. For the measurements, half of a hole was covered, whereas the exact amount of hole closure may vary during performance.

The embouchure hole is connected to the reference plane of the measurement system by a 3D-printed coupler, having the same inner geometry as the embouchure hole to ensure a good connection and sealing of the system. The dimensions of the *dizi* are listed in Appendix A 1.

It should be noted that only the linear behavior of the *dizi* is captured due to the small-amplitude sound source excitation. For the case of large jet flow in actual performance, nonlinear characteristics will likely be present though such behaviour is not considered in this study.

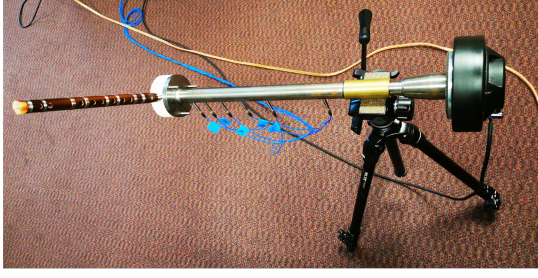


FIG. 2. Image of the impedance tube.

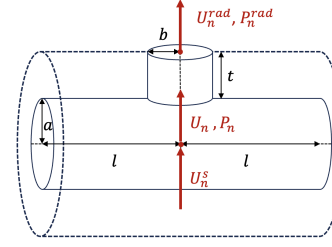


FIG. 3. Diagram of a single tonehole.

III. MODELING

A. Theory of TMM and TMMI

The assessment of a woodwind musical instrument's quality often involves analyzing the characteristics of its resonances, including the frequencies, magnitudes, and harmonicity. Additionally, the cutoff frequency of the tonehole lattice can provide valuable insights. These aspects can be inferred by examining the input impedance or reflectance of the instrument. The TMM offers an effective approach for computing the input impedance of the air column within the instrument.

The air column is modeled by breaking it down into a series of segments. These segments can take the form of cylinders, cones, and toneholes (either closed or open). Each segment is characterized by a Transfer Matrix (TM) that establishes the relationship between the input and output frequency-domain parameters, specifically pressure and volume flow. The overall response of the entire structure is then determined by multiplying the individual TMs in cascade. The impact of surface condition within the bore on the impedance spectra are investigated in Backus (1964) and Boutin *et al.* (2015, 2017), although this aspect is not considered in our study.

1. TMM

Using \mathbf{T}_i to represent the TM of the i th element, the system containing n elements can be expressed as

$$\begin{bmatrix} P_{in} \\ U_{in} \end{bmatrix} = \left(\prod_{i=1}^n \mathbf{T}_i \right) \begin{bmatrix} P_{out} \\ U_{out} \end{bmatrix}, \quad (1)$$

with P_{in} , U_{in} and P_{out} , U_{out} denoting input and output pressure and volume flow, respectively. $Z_{in} = P_{in}/U_{in}$ represents the input impedance, and $Z_R = P_{out}/U_{out}$ represents the radiation impedance at the end of the open pipe. The total TM of the system is $\mathbf{T}_{tot} = \prod \mathbf{T}_i$.

For a cylindrical duct, the TM is

$$\mathbf{T}_{cyl} = \begin{bmatrix} \cosh(\Gamma L) & Z_c \sinh(\Gamma L) \\ Z_c^{-1} \sinh(\Gamma L) & \cosh(\Gamma L) \end{bmatrix}, \quad (2)$$

where L is the length of the duct, $Z_c = \rho c/s$ is the characteristic impedance, c is the speed of sound, s is the cross-sectional area, and Γ is a complex propagation constant.

Γ can be written as (Van Walstijn *et al.*, 2005)

$$\Gamma = j\left(\frac{\omega}{c} + \alpha_\omega\right) + (\alpha_\omega + \alpha_c + \alpha_m), \quad (3)$$

where ω is radian frequency. α_ω , α_c , α_m are the attenuation constants associated with viscous drag and heat conduction at the tube wall, classical effects, and molecular effects, respectively (the detailed expressions are shown in Appendix B 1).

The elements of the TM of a conical duct \mathbf{T}_{cone} are (Lefebvre *et al.*, 2013)

$$\begin{aligned} \mathbf{T}_{cone}^{11} &= \frac{r_2}{r_1} \cos(k_c L) - \sin(k_c L)/k_c x_1, \\ \mathbf{T}_{cone}^{12} &= jZ_c \sin(k_c L), \\ \mathbf{T}_{cone}^{21} &= Z_c^{-1} [j(1 + (k_c^2 x_1 x_2)^{-1}) \sin(k_c L) + \\ &\quad (x_1^{-1} - x_2^{-1}) \cos(k_c L)/jk_c], \\ \mathbf{T}_{cone}^{22} &= \frac{r_1}{r_2} \cos(k_c L) + \sin(k_c L)/k_c x_2, \end{aligned} \quad (4)$$

where r_1 and r_2 are the radii at the input and output planes, respectively, and x_1 and x_2 are the distances between the apex of the cone and the input and output planes, $Z_c = \rho c/(\pi r_1 r_2)$ and $k_c = -j\Gamma$ is the complex wavenumber. In this case, losses are evaluated at the equivalent radius

$$r_{eq} = L \frac{r_1}{x_1} \frac{1}{\ln(1 + L/x_1)}. \quad (5)$$

The TM of a woodwind instrument's tonehole (Fig. 3) is written as (Keefe, 1982)

$$\begin{aligned} \mathbf{T}_{hole} &= \begin{bmatrix} 1 & Z_a/2 \\ 0 & 1 \end{bmatrix} \begin{bmatrix} 1 & 0 \\ 1/Z_s & 1 \end{bmatrix} \begin{bmatrix} 1 & Z_a/2 \\ 0 & 1 \end{bmatrix} \\ &= \begin{bmatrix} 1 + \frac{Z_a}{2Z_s} & Z_a(1 + \frac{Z_a}{4Z_s}) \\ 1/Z_s & 1 + \frac{Z_a}{2Z_s} \end{bmatrix}. \end{aligned} \quad (6)$$

The series and shunt impedances, Z_a and Z_s can be expressed in terms of equivalent lengths, which can be found in Appendix B 2.

2. TMMI

For woodwind instruments, there are often open holes in close proximity to one another. The TMM does

not account for possible external sound interactions between holes. The TMMI was proposed to incorporate the mutual radiation effect among openings, including open holes and the open end (Lefebvre *et al.*, 2013).

The bore is divided into two portions at the most upstream open hole, with the TMMI applied for the downstream portion of the air column to get the impedance seen by the most upstream hole. When calculating the upstream portion, it is essential to first consider a half-series impedance for the first open hole.

When the height of the tonehole is smaller than the wavelength, the pressure and velocity within the hole can be simplified as

$$\mathbf{P} = \mathbf{P}^{rad} + \mathbb{B}\mathbf{U} = \mathbb{Z}\mathbf{U}^{rad} + \mathbb{B}\mathbf{U} = (\mathbb{Z} + \mathbb{B})\mathbf{U}, \quad (7)$$

where \mathbf{P} , \mathbf{U} , \mathbf{P}^{rad} , and \mathbf{U}^{rad} are the pressure and volume flow at the hole inside the air column and chimney radiation surface, respectively, as shown in Fig. 3. \mathbb{B} is the impedance of the total acoustic mass of the hole, as seen in Appendix B3. \mathbb{Z} is the radiation impedance matrix, where the diagonal elements are self-impedances and the off-diagonal elements are mutual impedances.

The volume flow can be calculated by

$$\mathbf{U} = [\mathbb{I} + \mathbb{Y}(\mathbb{Z} + \mathbb{B})]^{-1}\mathbf{U}^s, \quad (8)$$

where \mathbb{I} is the identity matrix, and \mathbb{Y} is the admittance matrix, as seen in Appendix B3. A flow-source vector \mathbf{U}^s is introduced at each open hole for the calculation, which can be regarded as a virtual source. When we are only concerned with the impedance calculation, the virtual source is just a choice of reference. One solution is to apply only a reference volume flow to the left of the uppermost open hole. A pressure source is also a viable option.

The difference between the results of the TMM and TMMI becomes apparent as the number of openings increases and the frequency becomes higher. Therefore, using TMMI can provide more accurate results, especially when the relevant frequency range is above the cutoff frequency of the tonehole lattice. The modeling of the *dizi* using TMM and TMMI in this work is based on the Matlab toolbox *tmmt* (Scavone, 2021).

B. Matching volume length correction for the drilled toneholes

The matching volume length correction in Eq. (B13) is derived from the holes that protrude outwards from the tube, like flutes and saxophones. However, the toneholes of the *dizi* are directly drilled into the thick wall, similar to recorders. These two kinds of toneholes are referred to as protruded holes and drilled holes below. Thus, the matching volume is slightly different (Lefebvre, 2011; Rucz *et al.*, 2015). Lefebvre (2011) calculated the total equivalent length of the closed drilled hole, including the modified matching volume length correction, which is merged with the other length corrections and cannot be separated.

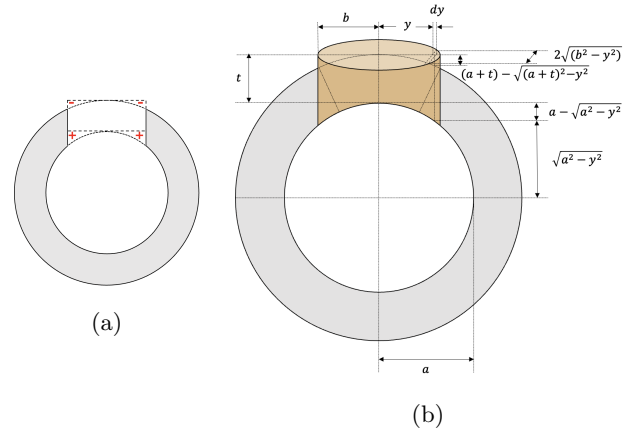


FIG. 4. Profile of a tonehole drilled in the thick wall.

Figure 4(a) is a section view of the drilled hole. For the volume correction of the protruded hole, only the volume indicated by red +’s needs to be added (Nederveen *et al.*, 1998), however, for the drilled hole, another volume indicated by red -’s should be removed from the top. Note that a further volume correction term should be taken into account during performance, as the finger penetrates some distance into the hole.

According to the geometric illustration of the drilled hole in Fig. 4(b), the matching volume can be calculated by integrating as

$$V_m^+ = \int_{-b}^{+b} 2\sqrt{b^2 - y^2} \left(a - \sqrt{a^2 - y^2} \right) dy, \quad (9)$$

and

$$V_m^- = - \int_{-b}^{+b} 2\sqrt{b^2 - y^2} \left(a + t - \sqrt{(a + t)^2 - y^2} \right) dy, \quad (10)$$

where a is the bore radius, b is the tonehole radius and t is the tonehole height. Then the total matching volume length correction can be expressed as

$$t_m^{(o/c)} = \frac{1}{\pi b^2} (V_m^+ + V_m^-). \quad (11)$$

Through numerical integration, it can be transformed into

$$t_m^{(o/c)} \approx \frac{tb^2}{8a(a + t)}. \quad (12)$$

C. Back end-holes

The back end-holes refer to two holes distributed radially along the *dizi*, as shown in Fig. 5. To the best of our knowledge, no one has provided a TM model for them. A similar structure could also be found on the *Xiao*, another Chinese air-jet driven woodwind instrument. When using TMM to model the *Xiao* in Lan and

Waltham (2016), the end-holes and the open end were treated together as a radiation impedance, which was obtained through measurement instead of modeling individually. The drawback of this approach is that it requires a measurement for each new instrument geometry.

Instead, the back end-holes can be approximated using an equivalent acoustic lumped model with a TM. As the dimensions of the two holes are nearly identical, they can be modeled as two parallel toneholes with the same parameters, which means doubling the series impedance and halving the shunt impedance. Due to the influence of the interaction between the internal and external interaction, slight differences in the impedance formula are reasonable. An empirically derived factor of 1/2.2 is applied instead of halving the shunt impedance, determined by matching theoretical results to measurements. This consideration is reasonable since mutual radiation between the two holes is also taken into account, as discussed in Appendix B 3.

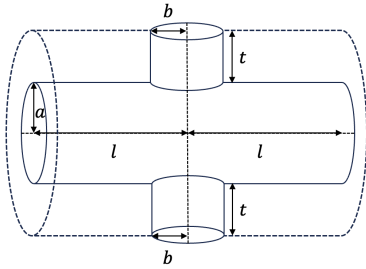


FIG. 5. Diagram of back end-holes.

D. Membrane hole

The equations of motion and the acoustic impedance for the *dizi* membrane are derived by Tsai (2003). The wrinkled membrane sealing on the tonehole can be modeled as a mass-spring system and its impedance can be expressed by

$$Z_{mem} = \frac{1}{S_m^2} \left[R + \frac{jm(\omega^2 - \omega_m^2)}{\omega} \right], \quad (13)$$

where m is the membrane mass, R is its damping coefficient and $\omega_m = 2\pi f_m$ is the resonant radian frequency. Then the membrane hole can be modeled through TM.

Tsai (2003) further emphasizes that both the resonance frequency and damping coefficient of the membrane undergo changes before and after impedance measurement. Due to fluctuations in membrane tension over time, the measured resonance frequency could exhibit variations of up to 15% between the initial and subsequent measurements. This variability has implications for accurately assessing the membrane's state, revealing its inherent instability. Musicians playing the *dizi* can distinctly perceive the instability in the membrane's condition during their performances. Therefore, by compar-

ing the impedance curves obtained from TMMI without the membrane to the measured curves with the membrane, the membrane parameters that produced the best fit for the measured *dizi* were found to be $f_m = 3.5$ kHz, $m = 8 \times 10^{-7}$ Kg and $R = 35 \times 10^{-4}$ Kg/s.

We model both the *dizi* with and without the membrane on the membrane hole. The former is considered as a closed hole, while the latter case is modeled with a closed-hole shunt impedance in series with the membrane impedance (with no mutual radiation between the membrane hole and other openings).

E. Upstream branch

When the embouchure hole of the *dizi* is considered as the input, the short duct between the cork and the embouchure hole, and the downstream main duct are connected in parallel. Therefore, it is necessary to rearrange the impedances.

Dickens (2007) mentioned that a measuring system imposes a discontinuity and alters the measured input impedance of flute headjoints, thus several small refinements are made to the model to improve the fit. A similar effect occurs in our measurements of the *dizi*. Therefore, a small length correction of $t_e = -1.7$ mm is applied to the embouchure hole to achieve closer fitting of impedance minima. Apart from that, a series resistance $R_{emb} = (6.9 \times 10^{-6} \text{ Hz}^{-1})fZ_c$ and a shunt conductance $G_{emb} = (1 \times 10^{-4} \text{ Hz}^{-1})f/Z_c$ are added at the input to get more accurate depth and height of impedance minima and maxima, respectively. Similar empirical refinements were used in Dickens (2007) and are based on an assumption that turbulence effects near discontinuities can be characterized as a dissipative process.

Figure 6 provides an equivalent circuit for this structure. The dashed-line boxes are used to group the components associated with the embouchure hole, the small duct, and refinements. Z_b is the impedance of the small duct. Z_w is the cork terminal impedance, which is approximated as being infinite, corresponding to a rigid wall. $Z(Z_R)$ is the impedance of the downstream main duct.

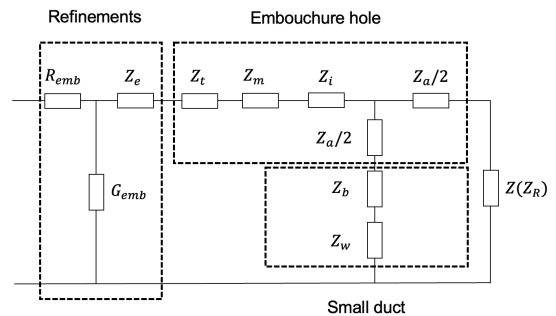


FIG. 6. Equivalent circuits representations for the upstream branch.

F. Results

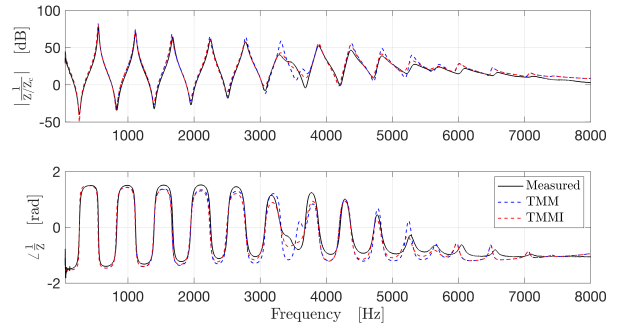
We have introduced all the elements necessary to model the entire *dizi* air column. The modeling results of the input admittance $1/Z_{in}$ magnitude and phase for the fingerings XXXXXX and XXXXOO, with and without membrane, are presented in Fig. 7. The black curves represent measurement data, the blue curves represent TMM data and the red curves represent TMMI data. Given that the frequencies near the minimum values of the input impedance curve are associated with the playing pitch for flute instruments, and the depth of the valley is presumed to correlate with the playability of the note, the admittance curves are displayed instead of the impedance curves for better observation. Hence, we focus on the maxima here. By comparison, it is quite obvious that the TMMI is a more accurate model than the TMM. This highlights the validity of considering external interactions.

IV. DISCUSSION

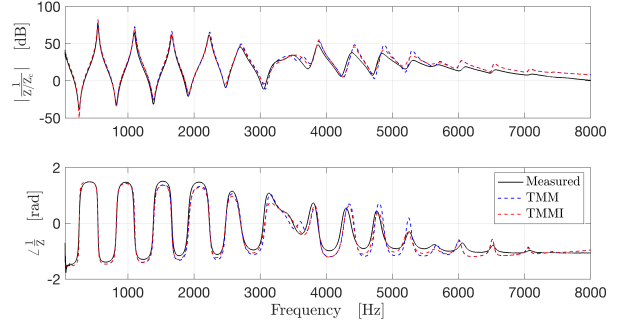
A. Input admittance

In order to analyze the overall characteristics of the *dizi*, the measured input admittances of all fingerings for the experiments, with and without the membrane are shown in Fig. 8. The top plots are the input admittance measurement curves of all fingerings for the *dizi* with membrane, using linear and decibel scales, respectively. The red plus signs are the maximum values obtained by a peak-finding algorithm. The peaks corresponding to the first three octaves from the middle plots are extracted and shown in the bottom scatter diagrams, taking the peak frequency as the abscissa, and the magnitude of the input admittance as the ordinate. The left side represents the *dizi* with the membrane, and the right side is without the membrane. The green, purple and blue dots correspond to the notes in the first, second and third octaves, respectively.

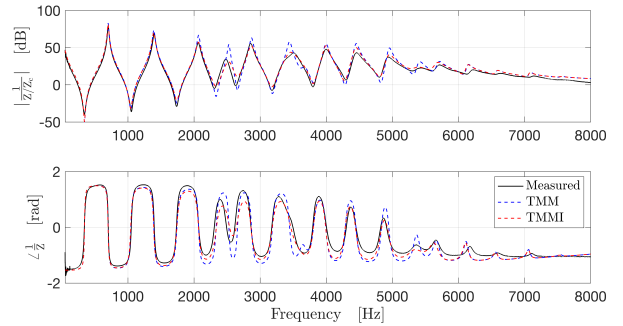
Looking at the top plots of Fig. 8, the F key *bangdi* can be divided into three frequency bands according to the characteristics of the input admittance curve: less than 2.3 kHz, 2.3 to 6 kHz, and greater than 6 kHz. In the first register below 2.3 kHz, the envelope of the input admittance curve drops relatively slowly, and the resonance becomes weaker with an increase in frequency, which is mainly caused by viscous-thermal losses. The frequency of the second register is 2.3 to 6 kHz, and the peak and valley values of the admittance are relatively reduced, which can be explained as the influence of the cutoff frequency of the tonehole lattice (Smith *et al.*, 2003), and agrees well with the cutoff frequency results in Sec. IV C. In addition, above the cutoff frequency, the effect of mutual radiation impedance is more obvious. The distortion around 3.5 kHz is due to the resonant frequency of the membrane. In the third register above 6 kHz, the input admittance curve suddenly becomes flat for each fingering. This behavior is characteristic of flute instruments



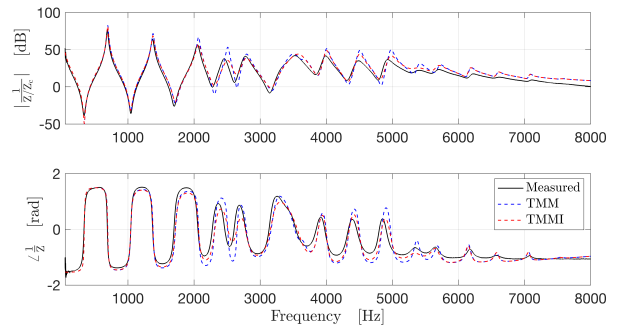
(a) Fingering XXXXXX, without membrane



(b) Fingering XXXXXX, with membrane



(c) Fingering XXXXOO, without membrane



(d) Fingering XXXXOO, with membrane

FIG. 7. Normalized input admittance magnitude and phase.

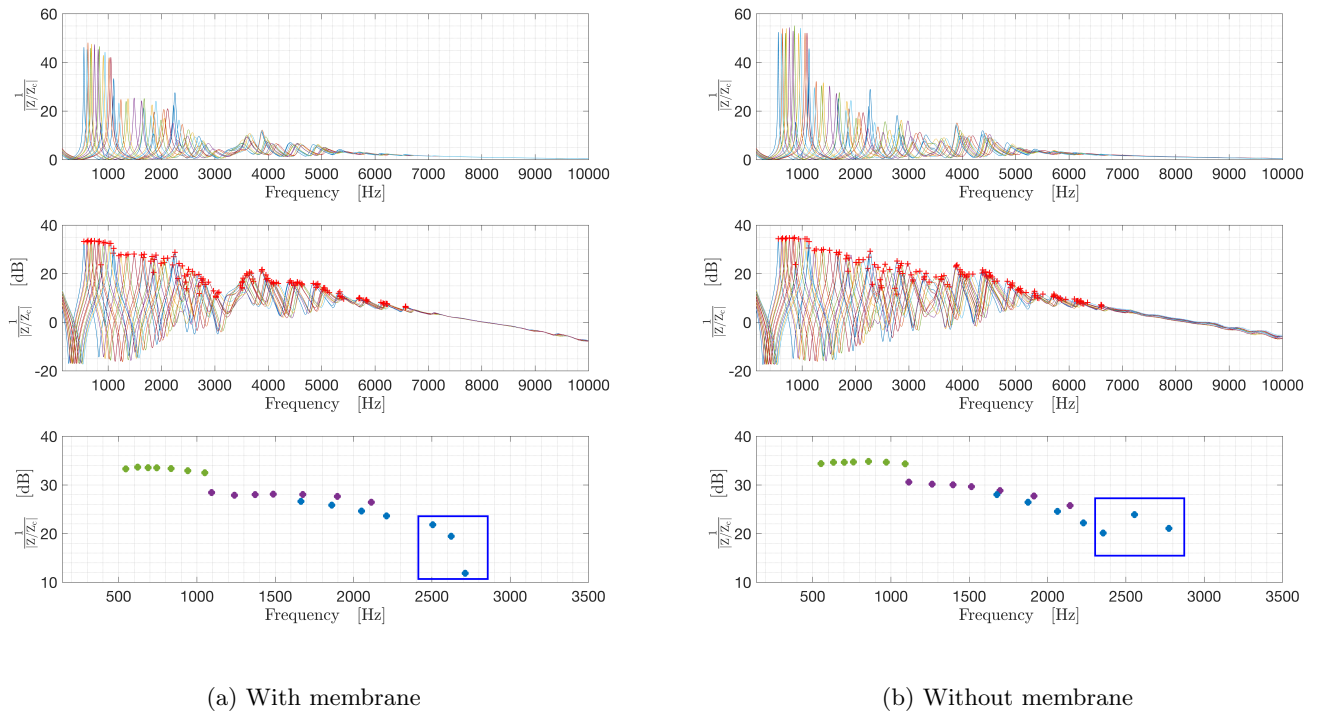


FIG. 8. Measurement input admittance results for all fingerings.

and is related to the Helmholtz shunt effect, as explained in Sec. IV C.

By extracting the admittance maximum values from the middle plots of Fig. 8, the data suggests that the presence of the membrane hole has a detrimental influence on the playability of the highest three notes with the corresponding fingerings XXOOOO, XOOOOO, and OOOOOO (in blue rectangular boxes). The reason for this phenomenon is due to the resonance frequency of the wrinkled membrane.

B. Membrane

As a particular component of the *dizi*, the wrinkled membrane that covers the membrane hole is believed to contribute to the unique sound character of the *dizi*. To study the influence of the membrane, the measured input admittance curves with and without the membrane are compared as shown in Fig. 9, corresponding to the XXXXXX fingering. The black curves represent the *dizi* without membrane, the red curves represent the *dizi* with membrane, and the first minima are zoomed in. It can be seen that the maximum value increases and the frequency decreases for the first octave when the membrane is attached, which are referred to as “resonance shifts” and “admittance reductions” (Tsai, 2003). The degree of the resonance shift and admittance reduction is related to the standing-wave pressure profile at the membrane hole location.

The TMM is used here to generate the pressure standing wave patterns to verify this relationship. A reference value should be defined at first to start calculating the pressure by TMM. In this work, the volume flow at the input is set to a constant value of one across all frequencies. Therefore, by dividing the *dizi* into several small segments (the length interval is less than 1.2 cm for each segment), the relative pressure of each position can be calculated.

To combine the resonance shifts and admittance reduction effects with the sound pressure change at the membrane hole for each fingering, Fig. 10 contrasts various extracted parameters¹. The frequencies and magnitudes of the first two maxima in the admittance curve are extracted for fingerings XXXXXX, XXXXO, XXXOO, XXXOOO, XOOOO, OOOOO, and OOOOOO, both with and without the membrane. Note that the notes corresponding to these fingerings are diatonic notes C5 to B6 for the first maximum and C6 to B7 for the second maximum. The top graph represents the frequency offset Δf of each note due to the membrane for C5-B6 (blue squares) and C6-B7 (red circles), expressed in cents. The second graph shows the frequency intervals of the octave, with (black squares) or without (pink circles) the membrane, expressed in cents. The reference value of 1200 cents, the octave in equal temperament is marked with a dashed line. The third figure shows the magnitude shifts $-\Delta|Z/Z_c|$ due to the membrane for C5-B6 (blue square) and C6-B7 (red circle). The last graph

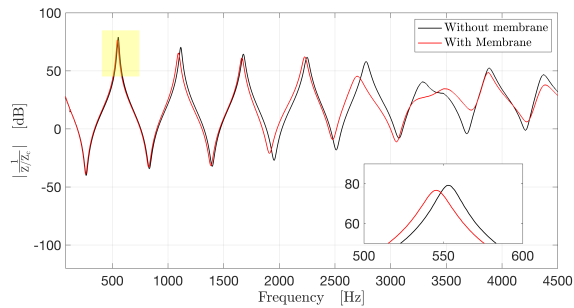


FIG. 9. Measured normalized admittance magnitude for fingering XXXXXX.

compares the relative sound pressure at the center of the membrane hole, with C5-B6 represented by blue squares and C6-B7 represented by red circles. Note that the data for the first three graphs are from measured data to ensure more accuracy, while the last graph is calculated using TMM.

From the overall comparison and analysis in Fig. 10, the blue curves for C5-B6 all tend to increase upward, while the red curves for C6-B7 all tend to decrease downward. From this, it can be concluded that there is a positive correlation between the sound pressure level at the membrane hole and the resonance shift and admittance reduction effects. On the other hand, it can be found that the octave shifts more for fingerings with more openings, leading to less accurate octaves for these fingerings. Moreover, as shown in the second graph, the octaves are more precisely tuned when the membrane is attached.

C. Upstream branch

The input impedance of the flute exhibits a sudden weakening around a specific frequency, attributed to the influence of the upstream branch as outlined in Smith *et al.* (2003). This phenomenon, known as the Helmholtz shunt, similarly occurs in the *dizi*.

In order to study the influence of the upstream branch, Figure 11 compares the input admittance and reflection coefficient $R = (Z_{in} - 1)/(Z_{in} + 1)$ curves modeled by the TMMI in the case of no membrane, with (black curves) or without (blue curves) an upstream branch, for fingering OOOOOO. Compared with the section marked in yellow, the upstream branch leads to a decrease in magnitude after 6 kHz, which is the Helmholtz shunt effect.

The cut-off frequency of the tonehole lattice can be estimated through the reflection coefficient (Petersen *et al.*, 2020). However, the upstream branch in flute instruments results in a more complex reflectance characteristic, which makes it harder to identify the cut-off frequency, as seen from the black curve in the red part of Fig. 11. Therefore, we suggest that when looking for the cut-off frequency of flute instruments, it is not necessary to consider the upstream branch. It is easy to find that

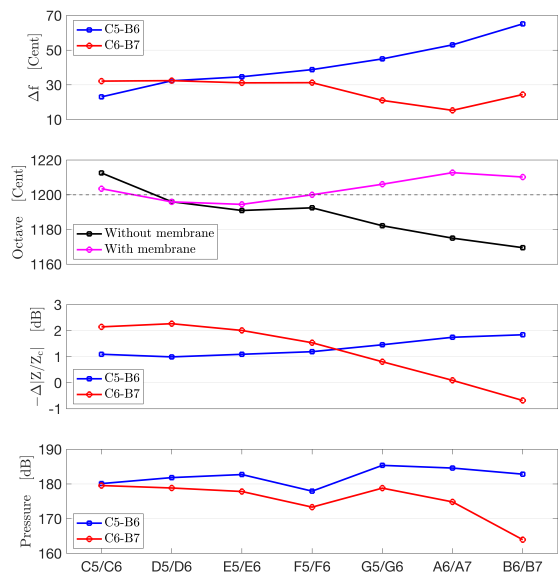


FIG. 10. Various extracted parameters comparison to illustrate membrane effect.

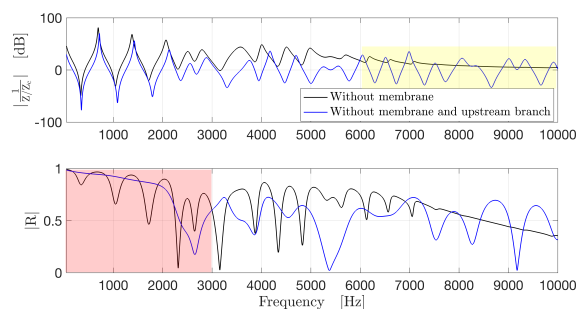


FIG. 11. Normalized admittance magnitude and reflection coefficient magnitude for fingering OOOOOO.

the cut-off frequency is between 2 to 3 kHz from the first minimum of the reflection coefficient curve for the *dizi* without the upstream branch, corresponding to the blue curve in Fig. 11.

V. CONCLUSION

In this study, we explore the acoustics of the Chinese transverse flute using input impedance measurements, modeling and analysis. Initially, the input impedance of an F key *bangdi* is measured for various fingerings.

Subsequently, both the TMM and TMMI are employed to model the air column of the *dizi*. Accurate characterization of the TM for each component is crucial in determining the behavior of both TMM and TMMI. Therefore, we provide specific TM derivations for the unique components of the *dizi*.

The correction for matching volume length differs between flanged and unflanged holes. Thus, considering the geometry, a numerical derivation for this term is presented. The two back end-holes, sharing similar dimensions and radially distributed along the bore, are modeled as two parallel toneholes with identical parameters. Additionally, the membrane's presence is regarded as an additional shunt impedance of the membrane hole. For a comprehensive understanding of the modeling of the upstream branch, an equivalent circuit is shown.

Through a comparative analysis of the modeling and measurement data, it becomes evident that the TMMI outperforms the TMM. This observation substantiates the rationale behind considering the mutual radiation impedance. Additionally, drawing from the measurement and modeling results, this study provides detailed acoustic analyses of the *dizi*.

The F key *bangdi* can be divided into three registers according to the characteristics of the input impedance curve: less than 2.3 kHz, 2.3 to 6 kHz, and greater than 6 kHz. By contrasting the impedance and pressure along the bore, it is confirmed that the membrane's location is related to the degree of resonance shift and admittance reduction effect. Consideration of the Helmholtz shunt effect leads us to reconsider the approach to determine the cutoff frequency of the tonehole lattice for flute instruments. Therefore, we suggest that excluding the upstream branch might be a good choice.

As part of future research directions, a more accurate numerical model for cylindrical mutual radiation and back end-holes can be studied. Furthermore, the non-linear behavior of the membrane and the excitation can be investigated and modeled.

APPENDIX A

1. Dimension of the bangdi in F

Table I and Table II provide the dimensions of the *bangdi* in F used in this manuscript, for the bore and toneholes, respectively. The center of the embouchure hole is regarded as the origin of the axial position, with the direction from the upstream to the downstream as the positive direction. The sequence of the toneholes is: embouchure hole, membrane hole, 6 finger holes, back end-holes, 2 front end-holes. It is worth noting that the dimensions for the back end-holes are for a single hole, as the shape of the two holes is identical with the same axial position.

TABLE I. Bore dimensions.

$x(mm)$	-10.60	0	17.40	42.40	57.40	82.40	100.40
$a(mm)$	7.1515	7.1895	7.2270	7.2815	7.3120	7.1080	7.0705
$x(mm)$	119.40	162.40	188.40	231.40	259.40	330.40	335.40
$a(mm)$	7.1390	6.9880	6.9430	6.7740	6.5990	5.8120	6.1910
$x(mm)$	335.40	345.80					
$a(mm)$	5.8125	5.8655					

TABLE II. Tonehole dimensions.

$x(mm)$	0	75.90	133.70	151.40	174.90	191.40	218.40
$b(mm)$	4.6830	3.6495	4.3315	4.2160	4.1925	4.1925	4.2160
$t(mm)$	3	3	3	3	3	3	3
$x(mm)$	243.70	288.35	299.90	316.40			
$b(mm)$	4.3545	4.3935	4.1895	4.1895			
$t(mm)$	3	3	3	3			

APPENDIX B

1. Propagation constant in a cylindrical tube

The following thermodynamic constants are given in (Keefe, 1984) for wave propagation in air:

$$\begin{aligned}
 \rho &= 1.179(1 - 0.00335\Delta T) \text{ Kg m}^{-3}, \\
 \mu &= 1.846 \cdot 10^{-5}(1 + 0.0025\Delta T) \text{ Kg s}^{-1} \text{ m}^{-3}, \\
 \gamma &= 1.4017(1 - 0.00002\Delta T), \\
 P_r &= \sqrt{0.8410(1 - 0.00002\Delta T)}, \\
 c &= 3.4723 \cdot 10^2(1 - 0.000166\Delta T) \text{ m s}^{-1},
 \end{aligned} \tag{B1}$$

where μ is the coefficient of viscosity, γ is the ratio of specific heats, P_r is the Prandtl number, and c is the wave velocity. These values are evaluated at $T_0 = 300$ °K (26.85 °C), and are accurate within ± 10 °K of that temperature. The temperature difference relative to T_0 is ΔT .

The expressions of the attenuation constants shown in (3) are

$$\alpha_\omega = \frac{1}{a} \sqrt{\frac{\omega\mu}{1\rho c^2}} \left[1 + \frac{\gamma - 1}{\sqrt{P_r}} \right], \tag{B2}$$

$$\alpha_c = \frac{\omega^2\mu}{2\rho c^3} \left[\frac{4}{3} + \frac{\mu_B}{\mu} + \frac{\gamma - 1}{P_r} \right], \tag{B3}$$

$$\alpha_m = \sum_\nu \frac{(\alpha_\nu\lambda)_m}{\lambda} \frac{2\omega\tau_\nu}{1 + (\omega\tau_\nu)^2}, \tag{B4}$$

where μ_B is the bulk viscosity, λ is the wavelength, and τ_ν is the relaxation times (ν indicates the type of gas molecule, dependent on humidity), $(\alpha_\nu\lambda)_m$ is the maximum absorption per wavelength associated with the ν -type relaxation process. The expressions of these terms can be found in Van Walstijn *et al.* (2005).

The physical parameters used in the modeling are: the room temperature is 20 °C, the relative room humidity is 40% and the atmospheric pressure is 101325 Pa.

2. Various impedances in TMM

The series impedance Z_a of the open and closed tonehole can be regarded as a small negative acoustic mass

$$Z_a^{(c/o)} = j \tan(kt_a^{(c/o)}) Z_c \approx j kt_a^{(c/o)} Z_c, \quad (\text{B5})$$

where the superscripts c and o stand for the closed and open tonehole, respectively, $k = 2\pi f/c$ is the lossless wave number, f is the frequency, $Z_c = \rho c/\pi a^2$ is the characteristic impedance of the bore radius a , ρ and c represent the density and the velocity of sound in air.

The calculation of the shunt impedance Z_s can be relatively complicated. For the closed hole, it is mainly represented by the acoustic compliance (Nederveen, 1969), given by Nederveen *et al.* (1998),

$$Z_s^{(c)} = j\{kt_i - \cot[k(t + t_m)]\} Z_c, \quad (\text{B6})$$

where t_i and t_m are the inner length and matching volume length correction, respectively.

Compared with the closed hole, $Z_s^{(o)}$ includes the radiation impedance, which can be expressed by the radiation length correction t_r (Dalmont *et al.*, 2002),

$$Z_s^{(o)} = j\{kt_i + \tan[k(t + t_m + t_r)]\} Z_c. \quad (\text{B7})$$

The expression of t_a, t_i is given from (Lefebvre and Scavone, 2012),

$$t_a^{(c)} = [-0.12 - 0.17 \tanh(2.4t/b)] b\delta^2, \quad (\text{B8})$$

$$t_a^{(o)} = [-0.35 + 0.06 \tanh(2.7t/b)] b\delta^2, \quad (\text{B9})$$

with $\delta = b/a$. The variable t_i can be expressed with a multiplicative factor $G(\delta, ka) = [1 + H(\delta)I(ka)]$ to account for frequency dependence,

$$t_i^{(c/o)} = (0.822 - 0.095\delta - 1.566\delta^2 + 2.138\delta^3 - 1.640\delta^4 + 0.502\delta^5) bG(\delta, ka), \quad (\text{B10})$$

where

$$H(\delta) = 1 - 4.56\delta + 6.55\delta^2, \quad (\text{B11})$$

and

$$I(ka) = 0.17ka + 0.92(ka)^2 + 0.16(ka)^3 - 0.29(ka)^4. \quad (\text{B12})$$

The matching volume length correction of the unflanged hole is shown here (Nederveen *et al.*, 1998)

$$t_m^{(o/c)} = \frac{b\delta}{1 + 0.207\delta^3}, \quad (\text{B13})$$

while the t_m used in the modeling of the *dizi* in this manuscript follows Eq. (12).

The radiation length correction of cylindrical flanges is given in Dalmont *et al.* (2001) and Lefebvre and Scavone (2012), which could be used for toneholes drilled through a thick wall,

$$t_r = 0.8216b - 0.47b[b/(a + t)]^{0.8}. \quad (\text{B14})$$

Since the wall thickness of the *dizi* is non-negligible, the end correction Z_r^L for a tube with an infinite flange is derived in Norris and Sheng (1989) and Dalmont *et al.* (2001).

$$\begin{aligned} Z_r^L &= [(1 + R_c)/(1 - R_c)] Z_c, \\ R_c &= -|R_\infty| e^{-2jk\delta_\infty}, \\ \delta_\infty &= 0.8216a \left[1 + \frac{(0.77ka)^2}{1 + 0.77ka} \right]^{-1}, \\ |R_\infty| &= \frac{1 + 0.323ka - 0.077(ka)^2}{1 + 0.323ka + (1 - 0.077)(ka)^2}. \end{aligned} \quad (\text{B15})$$

3. Matrix \mathbb{B} , \mathbb{Z} and \mathbb{Y} in TMMI

\mathbb{B} stands for the total acoustic mass of the open hole, which is a diagonal matrix, corresponding to the impedance with the length t and length corrections t_i and t_m . Its n th diagonal element is

$$B_{nn} = j\{kt_i + \tan[k(t + t_m)]\} Z_c. \quad (\text{B16})$$

The radiation matrix \mathbb{Z} includes both the self-radiation and mutual radiation impedance, with the diagonal elements representing self-radiation and the off-diagonal elements representing mutual radiation.

The self-radiation impedance of the n th opening for a tonehole is

$$Z_{nn} = j \tan(kt_r) Z_c. \quad (\text{B17})$$

The self-radiation impedance of the end follows Eq. (B15), $Z_{nn} = Z_r^{rad}$.

By assuming the open ends radiate as monopoles, the mutual radiation impedance Z_{nm} (when $n \neq m$) is (Pritchard, 1960)

$$Z_{nm} = jk\rho c \frac{e^{-jk d_{nm}}}{\epsilon \pi d_{nm}}, \quad (\text{B18})$$

where d_{nm} is the distance between open ends n and m , ϵ is a factor corresponding to the radiation space, $\epsilon = 2$ for a half space, and $\epsilon = 4$ for a complete space. As mentioned in Lefebvre *et al.* (2013), empirically it is difficult to determine the best approximation for the radiation impedance. They suggest to use $\epsilon = 2$ when the effect of interaction is especially important. In this manuscript, we use $\epsilon = 2$ between all axially distributed holes, and $\epsilon = 4$ between axially distributed holes and the end.

However, given the unique structure of the *dizi* with two radially distributed back end-holes, we need to define the mutual radiation impedance differently. We treat the back end-holes as a single component, as discussed in Sec. IIIC. In this scenario, the mutual radiation impedance between these holes and other openings is increased due

to the double radiation area; hence, we assume $\epsilon = 1$. Additionally, the mutual radiation between them is not taken into account because their mutual radiation effects have already been effectively considered through self-radiation. This implies that, from a physical standpoint, the shunt impedance includes contributions from both self-radiation and mutual radiation.

The admittance matrix \mathbb{Y} is related to the TM between two openings, corresponding to all the cascaded components between the two holes' shunt impedance Z_s or the end radiation impedance Z_r^L .

$$\begin{bmatrix} P_n \\ U_n \end{bmatrix} = \begin{bmatrix} A_n & B_n \\ C_n & D_n \end{bmatrix} \begin{bmatrix} P_{n+1} \\ U_{n+1} \end{bmatrix}, \quad (\text{B19})$$

which can be written in the form of an admittance matrix

$$\begin{bmatrix} U_n \\ U_{n+1} \end{bmatrix} = \begin{bmatrix} Y_n & Y_{\mu,n} \\ Y_{\mu,n} & Y'_n \end{bmatrix} \begin{bmatrix} P_n \\ P_{n+1} \end{bmatrix}, \quad (\text{B20})$$

where the relationship between the parameters is given by: $Y_n = D_n/B_n$, $Y'_n = A_n/B_n$ and $Y_{\mu,n} = -1/B_n$, which assumes that $A_n D_n - B_n C_n = 1$, the condition for reciprocity.

¹Figure 10 is the same as Fig. 9 in Luan *et al.* (2023). The legend labels for the second graph in Fig. 9 in Luan *et al.* (2023) are reversed. Please refer to the correct legend as provided in this paper.

- Backus, J. (1964). "Effect of wall material on the steady-state tone quality of woodwind instruments," *The Journal of the Acoustical Society of America* **36**(10), 1881–1887.
- Benade, A. H. (1990). *Fundamentals of musical acoustics* (Courier Corporation).
- Boutin, H., Le Conte, S., Fabre, B., and Le Carrou, J.-L. (2015). "Influence of the surface condition in the bore of woodwind instruments on the acoustic impedance," in *Cost FP1302 woodmusic-annual conference effects of playing on early and modern musical instruments*.
- Boutin, H., Le Conte, S., Vaedelich, S., Fabre, B., and Le Carrou, J.-L. (2017). "Acoustic dissipation in wooden pipes of different species used in wind instrument making: An experimental study," *The Journal of the Acoustical Society of America* **141**(4), 2840–2848.
- Caussé, R., Kergomard, J., and Lurton, X. (1984). "Input impedance of brass musical instruments—comparison between experiment and numerical models," *The Journal of the Acoustical Society of America* **75**(1), 241–254.
- Chaigne, A., and Kergomard, J. (2016). *Acoustics of musical instruments*, **10.1007/978-1-4939-3679-3** (Springer New York).
- Dalmont, J.-P., Nederveen, C. J., Dubos, V., Ollivier, S., Meserette, V., te Slighte, E. *et al.* (2002). "Experimental determination of the equivalent circuit of an open side hole: linear and non linear behaviour," *Acta Acustica united with acustica* **88**(4), 567–575.
- Dalmont, J.-P., Nederveen, C. J., and Joly, N. (2001). "Radiation impedance of tubes with different flanges: numerical and experimental investigations," *Journal of sound and vibration* **244**(3), 505–534.
- Dickens, P. (2007). "Flute acoustics: measurement, modelling and design," Ph.D. thesis, UNSW Sydney.
- Dickens, P., Smith, J., and Wolfe, J. (2007). "Improved precision in measurements of acoustic impedance spectra using resonance-free calibration loads and controlled error distribution," *The Journal of the Acoustical Society of America* **121**(3), 1471–1481.
- Keefe, and Douglas, H. (1990). "Woodwind air column models," *Journal of the Acoustical Society of America* **88**(1), 35–51.
- Keefe, D. H. (1982). "Theory of the single woodwind tone hole," *The Journal of the Acoustical Society of America* **72**(3), 676–687.
- Keefe, D. H. (1984). "Acoustical wave propagation in cylindrical ducts: Transmission line parameter approximations for isothermal and nonisothermal boundary conditions," *The Journal of the Acoustical Society of America* **75**(1), 58–62.
- Kemp, J. A., van Walstijn, M., Campbell, D. M., Chick, J. P., and Smith, R. A. (2010). "Time domain wave separation using multiple microphones," *The Journal of the Acoustical Society of America* **128**(1), 195–205.
- Kuang, W., Ji, P., Leistner, P., Angster, J., and Yang, J. (2016). "A physical model and sound synthesis method of chinese sheng," *ACTA ACUSTICA* **41**(5), 628–637.
- Lan, Y., and Waltham, C. (2016). "Acoustic modeling and optimization of the xiao," *Acta Acustica united with Acustica* **102**(6), 1128–1137.
- Lefebvre, A. (2011). "Computational acoustic methods for the design of woodwind instruments," Ph.D. thesis, McGill University.
- Lefebvre, A., and Scavone, G. P. (2011). "A comparison of saxophone a comparison of saxophone impedance and their playing behaviour," in *Proceedings of 2011 Forum Acusticum*, Aalborg, Denmark.
- Lefebvre, A., and Scavone, G. P. (2012). "Characterization of woodwind instrument toneholes with the finite element method," *The Journal of the Acoustical Society of America* **131**(4), 3153–3163.
- Lefebvre, A., Scavone, G. P., and Kergomard, J. (2013). "External tonehole interactions in woodwind instruments," *Acta Acustica united with Acustica* **99**(6), 975–985.
- Luan, X., Wang, S., Li, Z., and Scavone, G. (2023). "Acoustical Analysis of the Chinese Transverse Flute (dizi) using the Transfer Matrix Method," *Proceedings of Meetings on Acoustics* **49**(1), 035014.
- Nederveen, C., Jansen, J., and Van Hassel, R. (1998). "Corrections for woodwind tone-hole calculations," *Acta Acustica united with Acustica* **84**(5), 957–966.
- Nederveen, C. J. (1969). "Acoustical aspects of woodwind instruments," Ph.D. thesis, Technische Universiteit Delft.
- Ng, H. H., Tan, D., Ng, T., and Chen, J. (2021). "An acoustic impedance analysis of the dizi (chinese transverse flute)," in *27th International Congress on Sound and Vibration, ICSV 2021*.
- Norris, A., and Sheng, I. (1989). "Acoustic radiation from a circular pipe with an infinite flange," *Journal of Sound and Vibration* **135**(1), 85–93.
- Petersen, E., Turcotte, V., and Colinot, T. (2020). "Objective metrics to identify the tonehole lattice cutoff frequency of conical woodwind instruments," in *Forum Acusticum*.
- Plitnik, and George, R. (1979). "Numerical method for calculating input impedances of the oboe," *J.acoust.soc.am* **65**(3), 816.
- Pritchard, R. (1960). "Mutual acoustic impedance between radiators in an infinite rigid plane," *The Journal of the Acoustical Society of America* **32**(6), 730–737.
- Rossing, T. D., and Fletcher, N. H. (1991). *The physics of musical instruments* (Springer New York).
- Rucz, P., Augusztinovicz, F., Angster, J., Preukschat, T., and Miklós, A. (2015). "A finite element model of the tuning slot of labial organ pipes," *The Journal of the Acoustical Society of America* **137**(3), 1226–1237.
- Scavone, G. (2021). "A tutorial on the transfer matrix method for acoustic modeling," *The Journal of the Acoustical Society of America* **149**(4), A93–A93.
- Smith, J., Wolfe, J., and Green, M. (2003). "Head joint, embouchure hole and filtering effects on the input impedance of flutes," in *Proceedings of the Stockholm Music Acoustics Conference*.
- Tsai, C.-G. (2003). "The chinese membrane flute (dizi): physics and perception of its tones," Ph.D. thesis, Humboldt-Universität zu Berlin.
- Van Walstijn, M., Campbell, M., Kemp, J., and Sharp, D. (2005). "Wideband measurement of the acoustic impedance of tubular objects," *Acta acustica united with acustica* **91**(3), 590–604.
- Wang, S., Maestre, E., and Scavone, G. (2021). "Acoustical modeling of the saxophone mouthpiece as a transfer matrix," *The Journal of the Acoustical Society of America* **149**(3), 1901–1912.